



# Construction of heterostructured MIL-125/Ag/g-C<sub>3</sub>N<sub>4</sub> nanocomposite as an efficient bifunctional visible light photocatalyst for the organic oxidation and reduction reactions

Zhiwang Yang\*, Xueqing Xu, Xixi Liang, Cheng Lei, Yuhua Cui, Wenhua Wu, Yaxia Yang, Zhe Zhang, Ziqiang Lei\*

Key Laboratory of Polymer Materials of Gansu Province, Key Laboratory of Eco-Environment-Related Polymer Materials, Ministry of Education, College of Chemistry and Chemical Engineering, Northwest Normal University Lanzhou 730070, China

## ARTICLE INFO

### Article history:

Received 11 August 2016

Received in revised form 4 October 2016

Accepted 6 December 2016

Available online 7 December 2016

### Keywords:

Heterojunction photocatalyst

MIL-125

g-C<sub>3</sub>N<sub>4</sub> nanosheets

Ag NPs

Photocatalytic synthesis

## ABSTRACT

Photocatalytic synthesis using visible light is a desirable chemical process because of its potential to utilize sunlight. A heterostructured MIL-125/Ag/g-C<sub>3</sub>N<sub>4</sub> nanocomposite was implemented as an efficient bifunctional visible-light response catalyst for the photoreduction of nitrocompounds and the oxidation of alcohols. The photocatalyst was prepared via an accessible method and characterized by XRD, SEM, TEM, XPS, FT-IR, N<sub>2</sub> adsorption-desorption isotherm, UV-vis DRS, PL and EIS. The reactive efficiency of the photocatalyst depends on two primary factors, one is the light adsorption of catalysts, Ag nanoparticles (NPs) were photodeposited on the surface of g-C<sub>3</sub>N<sub>4</sub> and MIL-125 to increase visible-light absorption via the surface plasmon resonance. And the other is the separation efficiency of the photogenerated charge carrier. As an electron-conduction bridge in the interface between MIL-125 and g-C<sub>3</sub>N<sub>4</sub>, Ag NPs could facilitate the direct migration of photoinduced electrons from g-C<sub>3</sub>N<sub>4</sub> to MIL-125 and retard the recombination of electron-holes. Therefore, the MIL-125/Ag/g-C<sub>3</sub>N<sub>4</sub> sample shows highest photocatalytic activity compared with MIL-125, g-C<sub>3</sub>N<sub>4</sub>, MIL-125/Ag and MIL-125/g-C<sub>3</sub>N<sub>4</sub>. A corresponding photocatalytic mechanism of these reactions was discussed in detail. Moreover, the photoreduction of nitrocompounds and oxidation of the alcohols with superior conversions and selectivities were obtained, and the catalyst can be recycled four times. It is concluded that MIL-125/Ag/g-C<sub>3</sub>N<sub>4</sub> would be a promising visible light photocatalyst in the field of selective organic transformations.

© 2016 Elsevier B.V. All rights reserved.

## 1. Introduction

Metal organic frameworks (MOFs), also called porous coordination polymers (PCPs) are self-assemblies obtained via metal-oxide units joined by organic linkers through coordination bonds [1]. It was used for applications in H<sub>2</sub> storage [2], carbon dioxide capture [3] catalysis [4,5], optical materials [6] et al. Recent researches suggest that MOFs have the ability to behave as semiconductors when exposed to light [7,8], making them unique platforms for light harvesting and photoinduced catalysis [9–11] for hydrogen evolution [6], carbon dioxide reduction [12], degradation of the organic pollutants [9] and transformation of organic compounds [13]. A case in point, MIL-125 (MIL = Materials of Institut Lavoisier)

is composed of basic units of Ti<sub>8</sub>O<sub>8</sub>(OH)<sub>4</sub>-(O<sub>2</sub>C-C<sub>6</sub>H<sub>5</sub>-CO<sub>2</sub>)<sub>6</sub>, constructed from corner or edge sharing octahedral titanium units and leaded to a porous three-dimensional quasi-cubic tetragonal structure [14]. Nevertheless, pure MIL-125(Ti) has a bad gap within ultraviolet region at about 3.6 eV. So it is related to the reduction of Ti (IV) to Ti (III) under UV irradiation, which accounts for only 3–5% of the solar spectrum [15]. Therefore, it is extremely important to develop the visible light responded MIL-125 based catalysts. Numerous attempts have been dedicated to increasing the photocatalytic efficiency of MIL-125. For example, noble metal deposition [16], coupled with inorganic semiconductor [17] and introduction of organic chromophores, NH<sub>2</sub>, in the linker [18] et al. To date, the heterostructures integrating MOFs with other functional materials such as CdS [19], Fe<sub>3</sub>O<sub>4</sub> [20], ZnO and C<sub>3</sub>N<sub>4</sub> [21] etc acted as catalysts show great advantages due to their synergism effect [22]. Especially, graphitic carbon nitride (g-C<sub>3</sub>N<sub>4</sub>) [23,24], a metal-free polymer semiconductor, possesses stacked two-dimensional struc-

\* Corresponding authors.

E-mail addresses: [yangzw@nwnu.edu.cn](mailto:yangzw@nwnu.edu.cn) (Z. Yang), [leizq@nwnu.edu.cn](mailto:leizq@nwnu.edu.cn) (Z. Lei).

ture, with tris-triazine building units connected with planar amino groups in each layer and weak van der Waals force between layers. It has attracted a focus of attention for photocatalytic reactions, because this material is cheap, easy to synthesize, and environmental friendly [25,26]. It is more important that g-C<sub>3</sub>N<sub>4</sub> owns relatively narrow band gap of 2.45 eV and the energy position of CB and VB is at -0.85 and 1.6 eV vs normal hydrogen electrode (NHE), respectively [27]. More recently, Hou W and his colleagues was reported that g-C<sub>3</sub>N<sub>4</sub>/MIL-125 heterostructured photocatalyst exhibited an improved photocatalytic performance for the degradation of Rhodamine B under visible-light irradiation [28]. Nonetheless, bulk g-C<sub>3</sub>N<sub>4</sub> suffers the predicament of limited photocatalytic activity due to low quantum yield and high recombination rate of photo-generated charges [29]. Recent research shows that layer g-C<sub>3</sub>N<sub>4</sub> nanosheets with high specific surface area exhibit many intriguing properties different from bulk g-C<sub>3</sub>N<sub>4</sub>. Therefore, the g-C<sub>3</sub>N<sub>4</sub> nanosheets could effectively improve the photocatalytic activity.

Besides, it is well-known that for semiconductor-based photocatalysts, the separation efficiency of the photogenerated charge carriers is an important factor in determining their photocatalytic performance [30]. To further overcome the fast recombination process of the photocatalyst, considerable researches have been carried out using a noble metallic combination of semiconductors [31,32]. Ag nanoparticles (Ag NPs) can act as efficient electrons traps to suppress photoinduced electron-hole recombination at a certain extent. In addition, Ag NPs formed on the surface of semiconductors could strongly absorb visible light because of the surface plasmon resonance of Ag atom [22,33,34].

Based on the above discussion, to improve the photocatalytic activity of the MIL-125, herein we report a new hybrid photocatalyst made by heterostructured MIL-125/Ag/g-C<sub>3</sub>N<sub>4</sub> nanocomposite. It was primarily focused on its dual applications in the photocatalytic synthesis including the reduction of nitrocompounds into aromatic amine and the selective oxidation of alcohols.

The green chemistry involving photocatalytic synthesis, where photon is used as one of the reactants of chemical reactions, is a growing field. Moreover, the photocatalytic oxidation and reduction progress have carried out using the mild experimental conditions [35,36]. For example, photocatalytic reduction of nitrobenzene into aniline using photocatalytic technology has been reported in some literatures [37,38]. Theoretically, when the conduction band (CB) potential of photocatalyst is lower than -0.486 V, nitrobenzene (NB) can be photocatalytically reduced into aniline (AN) ( $E(C_6H_5NO_2/C_6H_5NH_2) = -0.486$  V, vs NHE), the methanol or isopropyl alcohol provide the proton and the photoinduced electrons were used as the reducing agent, so the whole process is eco-friendly and economical. Moreover, aromatic nitro-compounds reduction will produce aromatic amines that are valuable intermediate materials for production of dyes, pharmaceuticals, agro-chemicals, cosmetics, and chelating agents [39]. Therefore, photocatalytic reduction of nitrobenzene into aniline is significant. Again for instance, aromatic aldehydes and their derivatives are important fine chemical intermediate. Nowadays, photocatalytic aerobic alcohols to the aldehydes or ketones with molecular oxygen as oxidant have caused the extensive concern. Because, its providing of an economical and green way for this type of transformation [18,40].

According the experimental results, it was found that the MIL-125/Ag/g-C<sub>3</sub>N<sub>4</sub> composite has exhibited much higher photocatalytic activity for reduction of nitrobenzene into aniline and aerobic alcohols to the aldehydes or ketones than the bare MIL-125 or g-C<sub>3</sub>N<sub>4</sub> under visible-light irradiation (>400 nm), distinctly demonstrating that the existence of a synergistic effect among Ag, g-C<sub>3</sub>N<sub>4</sub> and MIL-125. The low recombination of the photoinduced electron-holes of the prepared MIL-125/Ag/g-C<sub>3</sub>N<sub>4</sub> nanocomposites was confirmed based on a photoluminescence (PL) and electro-

chemical impedance spectroscopy (EIS) technique. In addition, the possible photocatalysis mechanism of MIL-125/Ag/g-C<sub>3</sub>N<sub>4</sub> under visible light was also discussed.

## 2. Experimental

### 2.1. Materials

All the used reagents and solvents were analytical grade and received from commercial sources without further purification. Titanium isopropoxide (Ti(O-iPr)<sub>4</sub>), 1,4-benzenedicarboxylic acid (H<sub>2</sub>BDC), benzyl alcohol, 4-methoxybenzyl alcohol were obtained from Aladdin Reagent Co., Ltd. N,N-dimethylformamide (DMF), melamine (C<sub>3</sub>H<sub>6</sub>N<sub>6</sub>), concentrated hydrochloric acid (HCl, 36.0–38.0%), polyethylene glycol (PEG2000) and silver nitrate (AgNO<sub>3</sub>) were obtained from Shanghai Fine Chemical Materials Research Institution. 4-Nitrobenzyl alcohol, 2-methylbenzyl alcohol, 4-chlorobenzyl alcohol 2-methoxybenzyl alcohol, 4-hydroxybenzyl alcohol, benzhydrol, 4-chlorobenzhydrol, and 4-methoxybenzhydrol were obtained from the Beijing J&K Scientific Co. Ltd. 4-Methylbenzyl alcohol, 4, 4'-dimethylbenzhydrol, 4, 4'-dimethoxybenzhydrol and 4, 4'-dichlorobenzhydrol were obtained from Alfa Aesar Co. Ltd. Nitrobenzene and its derivatives were obtained from Aladdin Reagent Co., Ltd. or Beijing J&K Scientific Co., Ltd.

### 2.2. Preparation of photocatalysts

#### 2.2.1. Synthesis of MIL-125

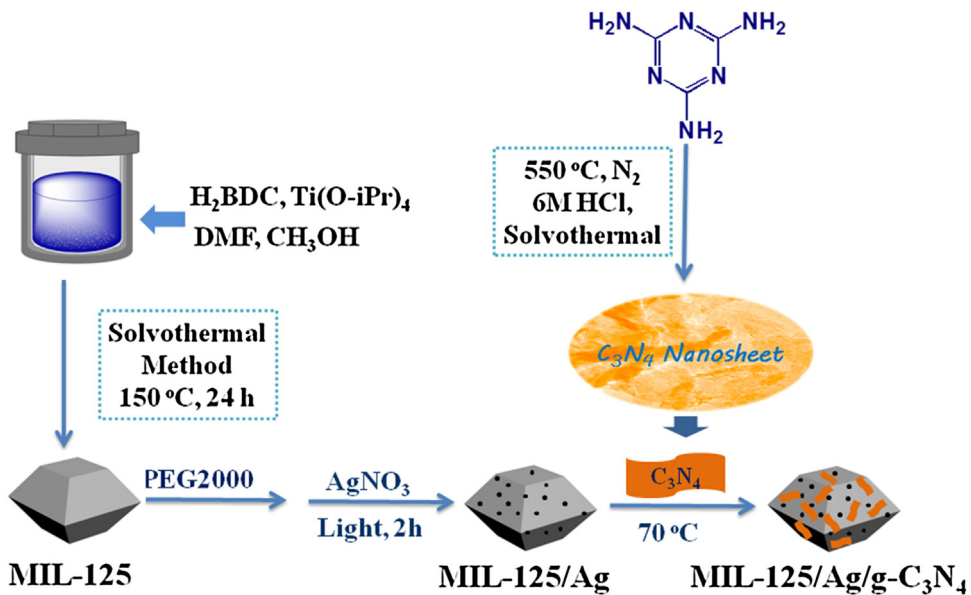
MIL-125 was synthesized according to the literature [41]. In a typical synthesis procedure, a mixture of Ti(O-iPr)<sub>4</sub> (1.60 mL), H<sub>2</sub>BDC (3.00 g), 6 mL of CH<sub>3</sub>OH and 56 mL of DMF were stirred at room temperature until it become a clear solution, then it was transferred into a 100 mL Teflon liner. After that, it was sealed in a stainless steel autoclave and heated at 150 °C for 48 h. The resultant suspension was filtered, washed with DMF and C<sub>2</sub>H<sub>5</sub>OH, respectively. The white powder was collected by filtering and drying under vacuum at 100 °C for 12 h.

#### 2.2.2. Synthesis of g-C<sub>3</sub>N<sub>4</sub> nanosheets

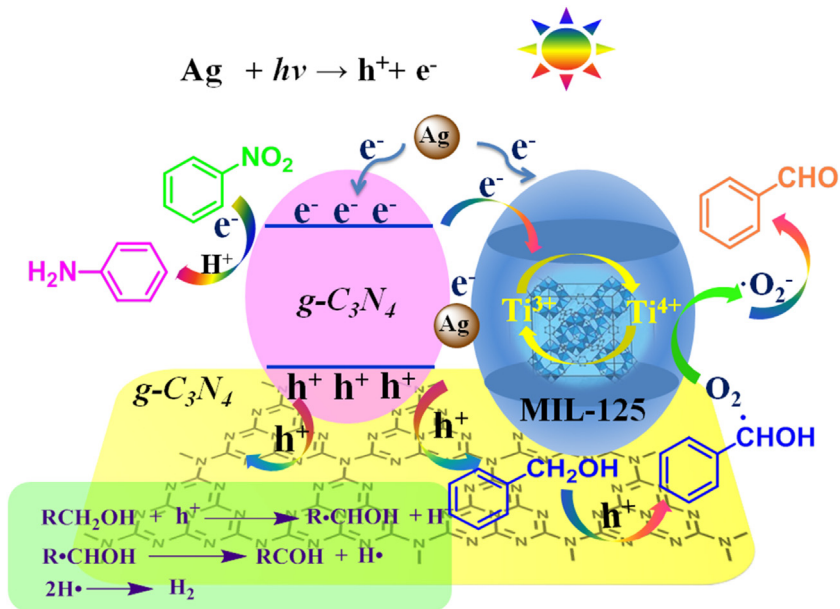
Graphite-like C<sub>3</sub>N<sub>4</sub> (g-C<sub>3</sub>N<sub>4</sub>) were synthesized on the basis of a procedure reported [33,42]. Specifically, 5.0 g of melamine was heated from room temperature to 550 °C with a heating rate of 3 °C/min and then calcined at 550 °C for 4 h in a N<sub>2</sub> furnace. The obtained yellow agglomerate was ground into powder. 1.0 g of the above powder was dispersed in 60 mL of 6 M HCl solution string for 1 h for protonation of g-C<sub>3</sub>N<sub>4</sub>. Then the suspension was transferred into a 100 mL Teflon liner. Then it was sealed in a stainless steel autoclave and heated at 120 °C for 8 h. After cooled down to the room temperature, the suspension was filtered, washed with deionized water until the filtrate was close to neutral conditions. The collected g-C<sub>3</sub>N<sub>4</sub> was dried at 100 °C in vacuum for 4 h. In order to conveniently use of the as-prepared g-C<sub>3</sub>N<sub>4</sub> subsequently, 100 mg of the protonated g-C<sub>3</sub>N<sub>4</sub> was ultrasonically dispersed in 100 mL of deionized water for 4 h to form a stable suspension of g-C<sub>3</sub>N<sub>4</sub> nanosheets.

#### 2.2.3. Synthesis of MIL-125/Ag/g-C<sub>3</sub>N<sub>4</sub> nanocomposite

A series of MIL-125/Ag/g-C<sub>3</sub>N<sub>4</sub> nanocomposite with different mass ratios of MIL-125 vs g-C<sub>3</sub>N<sub>4</sub> nanosheets were synthesized by a facile method as follows, the as-prepared MIL-125 power (200 mg) was mixed with 100 mL of deionized water by ultrasonication for 30 min. Then 1.0 mL of 5% PEG2000 was added and the dispersion was stirred for another 30 min. To deposit the Ag NPs on the surface of the MIL-125, a photodeposition method was applied. Firstly,



**Scheme 1.** The illustration for the preparation of MIL-125/Ag/g-C<sub>3</sub>N<sub>4</sub> photocatalyst.



**Scheme 2.** The proposed mechanism for the photocatalytic process by MIL-125/Ag/g-C<sub>3</sub>N<sub>4</sub>.

4.0 mL of AgNO<sub>3</sub> solution (2.0 mg mL<sup>-1</sup>) was added to the above dispersion for the MIL-125. Then the suspension was transferred to a water-cooled reactor (250 mL) and irradiated under a 500 Xe lamp for 2 h. For further wrapping of g-C<sub>3</sub>N<sub>4</sub> on MIL-125/Ag, a certain amount (6, 12 and 18 mL, respectively) of the protonated g-C<sub>3</sub>N<sub>4</sub> nanosheets solution (1 mg mL<sup>-1</sup>) was added and the reaction temperature was kept at 70 °C for 120 min. When cooled down to the room temperature, the resulting suspension was filtered, washed with deionized water and C<sub>2</sub>H<sub>5</sub>OH three times sequentially, and dried at 60 °C for 24 h in a vacuum oven. The finally products were named MIL-125/Ag/C<sub>3</sub>N<sub>4</sub>(x) (x=6, 12 and 18; x represents the volume of the g-C<sub>3</sub>N<sub>4</sub> nanosheets solution). For comparison, MIL-125/Ag and MIL-125/g-C<sub>3</sub>N<sub>4</sub> were also prepared according the above methods. Besides, the whole process for the preparation of the catalyst was presented in the Scheme 1.

### 2.3. Characterization

The Fourier transform-infrared spectroscopy (FT-IR) was carried on a Nicolet NEXUS 670 spectrometer using KBr disks in the scanning range of 4000–400 cm<sup>-1</sup>. The powder X-ray diffraction (XRD) was carried on a Rigaku D/Max-2400 diffractometer with Cu K $\alpha$  radiation ( $\lambda = 1.5418 \text{ \AA}$ ). UV-vis diffuse reflectance spectra (UV-vis DRS) were obtained by a Cary 500 UV-vis-NIR spectrophotometer. The photoluminescence spectra (PL) were conducted on a PELS-55 luminescence fluorescence spectrophotometer. The morphology of the samples were characterized by field emission scanning electron microscopy (FE-SEM, Ultra Plus, Carl Zeiss, Germany). Transmission electron microscopy (TEM) was measured using a JEOL model JEM2010 EX microscope at an accelerating voltage of 200 kV. A XPS (ThermoVG Scientific Sigma Probe) using an Al K $\alpha$  radiation was used to study the surface compositions of the

catalysts. Electrochemical impedance spectroscopy (EIS) was performed on an electrochemical CHI660B workstation (Shanghai Chenhua, Inc.). The products of the selective oxidation of alcohols and the reduction of the nitrocompounds were recorded through gas chromatograph (GC) analyses on a Shimadzu GC-2010 equipped with a RTX-1 capillary column and a FID detector.

#### 2.4. Photocatalytic experimental details

In the photocatalytic activity test, aryl alcohol (0.2 mmol) or aromatic nitro compounds solution (0.1 mmol) was dissolved in a solution of 6 mL of solvent in the presence of 5 mg catalyst in an open quartz tube and the suspension was stirred in the dark for 1 h to ensure the establishment of adsorption-desorption equilibrium. A 500 W Xe lamp ( $\lambda > 400$  nm) (PLS-SXE 300, BiLon Co. Ltd., Shanghai China) with a 400 nm cutoff filter was used as the visible-light source. Then the reaction mixture was irradiated for appropriate time under room temperature. The whole reduction or oxidation experimental process was conducted under  $N_2$  or  $O_2$  atmosphere, respectively. After reaction, the conversion and the selectivity were recorded on a gas spectrometry. During the process of the reduction of NB reaction, 2 mL of sample solution was collected at a certain time interval from one of the several parallel reactions and centrifuged to remove the catalyst completely at 8000 rpm. And 50  $\mu$ L of the reaction solution was added to 5 mL of deionized water. Afterward, the transparent solution was analyzed on a Varian ultraviolet-visible light (UV-vis) spectrophotometer (Cary-50, Varian Co.).

#### 2.5. Electrochemical measurements

Electrochemical impedance spectroscopy (EIS) tests were carried out with AC impedance-potential model in a standard three-electrode system. Namely, a saturated calomel electrode (SCE) as a reference electrode, a Pt foil as the counter electrode, and MIL-125/Ag/g-C<sub>3</sub>N<sub>4</sub> as the working electrodes. The progress was performed under dark condition at open circuit potential over the frequency range between  $10^5$  and  $10^{-2}$  Hz, with an AC voltage magnitude of 5 mV in 0.2 M Na<sub>2</sub>SO<sub>4</sub> solution. For the preparation of composite electrodes, MIL-125 based composites were dispersed in chitosan solution to form a 5 mg mL<sup>-1</sup> solution and ultrasonicated for 30 min, then 0.1 mL of colloidal solution was dropped on the conductive side of the FTO glass and allowed to dry at room temperature and 100 °C in the air for 24 h.

### 3. Results and discussion

#### 3.1. Characterization

The XRD patterns for the bulk g-C<sub>3</sub>N<sub>4</sub>, g-C<sub>3</sub>N<sub>4</sub> nanosheets, MIL-125/Ag, MIL-125/C<sub>3</sub>N<sub>4</sub> and MIL-125/Ag/g-C<sub>3</sub>N<sub>4</sub> series with different weight contents of g-C<sub>3</sub>N<sub>4</sub> nanosheets are shown in Fig. 1. The diffraction peaks of the MIL-125 can be well matched with the previous reported and simulated one [12,43]. It is indicated that the MIL-125 was synthesized successfully. In the spectrogram of the bulk g-C<sub>3</sub>N<sub>4</sub> and g-C<sub>3</sub>N<sub>4</sub> nanosheets, both of them have two characteristic peaks at 27.5° and 13.1° respectively. The strong XRD peak at 27.5° is typically corresponds to the (002) diffraction plane, which is well-known for the melon networks. While the latter with a much weaker intensity at 13.1° is attributed to (100) in-plane [44]. For the g-C<sub>3</sub>N<sub>4</sub> nanosheets, the XRD pattern shows a significant intensity increase of the (002) diffraction plane of the g-C<sub>3</sub>N<sub>4</sub>. Meanwhile, for the MIL-125/g-C<sub>3</sub>N<sub>4</sub>, compared to the XRD patterns of MIL-125, the (002) plane of the g-C<sub>3</sub>N<sub>4</sub> were observed on the MIL-125/g-C<sub>3</sub>N<sub>4</sub>. For the MIL-125/Ag, the XRD pattern was similar to that of MIL-125. Besides, owing to the small amount of

metallic Ag in the composites, only a weak (111) diffraction plane of Ag NPs detected at 38.1°. It is suggested that silver atoms are not incorporating into the MIL-125 [45] (Fig. 1a). Moreover, For the MIL-125/Ag/g-C<sub>3</sub>N<sub>4</sub> (Fig. 1b), both the plane of Ag NPs and the (002) crystal plane of g-C<sub>3</sub>N<sub>4</sub> were also could be found in all the MIL-125/Ag/g-C<sub>3</sub>N<sub>4</sub> patterns. In conclusion, the g-C<sub>3</sub>N<sub>4</sub> and Ag NPs were successfully attached on the surface of the MIL-125. Moreover, characteristic peaks of the MIL-125 were also remained in all samples. It is demonstrated that the structure of the MIL-125 was unchanged.

The existence of g-C<sub>3</sub>N<sub>4</sub> and Ag NPs in the as-prepared samples was further confirmed by FT-IR analysis. In Fig. 2a, for MIL-125, the large broad absorption band centered at 3500 cm<sup>-1</sup> can be assigned to the free solvent molecules trapped within the adsorbent pores. The strong bands at 1646 and 1400 cm<sup>-1</sup> are signed to the vibrational stretching frequencies of the framework (O—C—O) which confirm the presence of the dicarboxylate linker in the MIL-125 framework. Characteristic absorption of benzene rings can be located at 1013 and 740 cm<sup>-1</sup>. The bands at 670 cm<sup>-1</sup> is attributed to the in-plane and out-of-plane bending modes of —COO groups. The bands between 400 and 800 cm<sup>-1</sup> are attributed to (O—Ti—O) vibrations [46]. For the g-C<sub>3</sub>N<sub>4</sub>, three main absorption regions can be observed clearly. The broad peak at 3000–3500 cm<sup>-1</sup> is ascribed to the stretching vibration of N—H and O—H of the physically adsorbed water. The strong bands of 1200–1700 cm<sup>-1</sup>, with the characteristic peaks at 1240, 1320, 1407, 1567, and 1640 cm<sup>-1</sup>, are attributed to the typical stretching vibration of C—N heterocycles [47]. The MIL-125/Ag and MIL-125/g-C<sub>3</sub>N<sub>4</sub> composites show similar absorption bands to the pure MIL-125. Furthermore, for the MIL-125/Ag/g-C<sub>3</sub>N<sub>4</sub> (Fig. 2b), it can be also seen clearly that the main characteristic peaks in the MIL-125 spectrum are also observed in the MIL-125/Ag/g-C<sub>3</sub>N<sub>4</sub> compounds. At the same time, the original characteristic peaks at 1200–1000 cm<sup>-1</sup> in the MIL-125 become a broad band centered at 1100 cm<sup>-1</sup> in MIL-125/Ag/g-C<sub>3</sub>N<sub>4</sub>. It is indicated that interaction force among the MIL-125, Ag NPs and C<sub>3</sub>N<sub>4</sub> were existed. Therefore, the chemical structure of MIL-125/Ag/g-C<sub>3</sub>N<sub>4</sub> is successfully prepared.

X-ray photoelectron spectroscopy (XPS) measurements were carried out to elucidate the surface composition and the chemical states of the elements (Fig. 3). The survey XPS spectrum (Fig. 3a) for MIL-125/Ag/g-C<sub>3</sub>N<sub>4</sub> indicates that the composite mainly consists of C, N, O, Ti, and Ag atoms, with the surface contents of 57.6%, 2.0%, 33.4%, 6.7% and 0.36%, respectively. They are well consistent with the chemical compositions. To gain more insight into the chemical bonding among these atoms in the composite, the high resolution XPS spectra of C 1s, N 1s, Ti 2p, O 1s and Ag 3d were deconvoluted by Gaussian-Lorenzian analysis method. For C 1s spectra (Fig. 3b), three distinct peaks at 284.6, 285.9 and 288.6 eV are observed. The first peak is attributed to sp<sup>2</sup> carbon in g-C<sub>3</sub>N<sub>4</sub> and benzoic rings, the second one is ascribed to the C—NH<sub>2</sub> species on the g-C<sub>3</sub>N<sub>4</sub>. The last one is the sp<sup>2</sup> hybridized carbon in N-containing aromatic ring (N—C=N) [48]. For N 1s spectra (Fig. 3c), three fitted peaks are observed to locate at around 398.7, 399.7, 401.3 eV, respectively. These peaks can be regarded as the sp<sup>2</sup> hybridized nitrogen involved in triazine rings (C—N=C), the tertiary nitrogen N—(C)<sub>3</sub> groups, and the free amino groups (N—H), respectively [49]. The O 1s spectra of MIL-125/Ag/g-C<sub>3</sub>N<sub>4</sub> shown in Fig. 3d can be split into three peaks. The peak at 532.3 eV is assigned to the OH group [47]. The peaks at 531.7 and 529.7 eV can be ascribed to C=O and titanium-oxo cluster, respectively [50]. Fig. 3e shows Ti 2p spectra. The binding energy values of Ti 2p<sub>3/2</sub> and Ti 2p<sub>1/2</sub> were allocated at 458.8 and 464.3 eV, respectively, indicating that titanium bounded to oxygen remains in oxidation state of Ti (IV) for the titanium-oxo cluster [28]. Fig. 3f presents the high-resolution Ag 3d doublets with binding energies situated at 368.2 and 374.4 eV which were

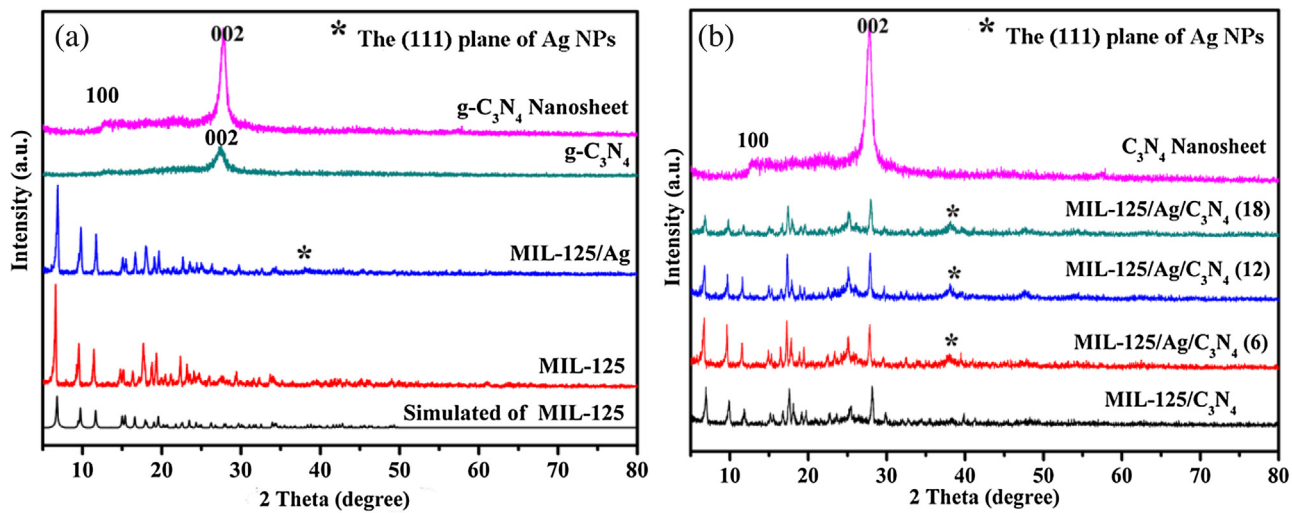


Fig. 1. PXRD patterns of the samples.

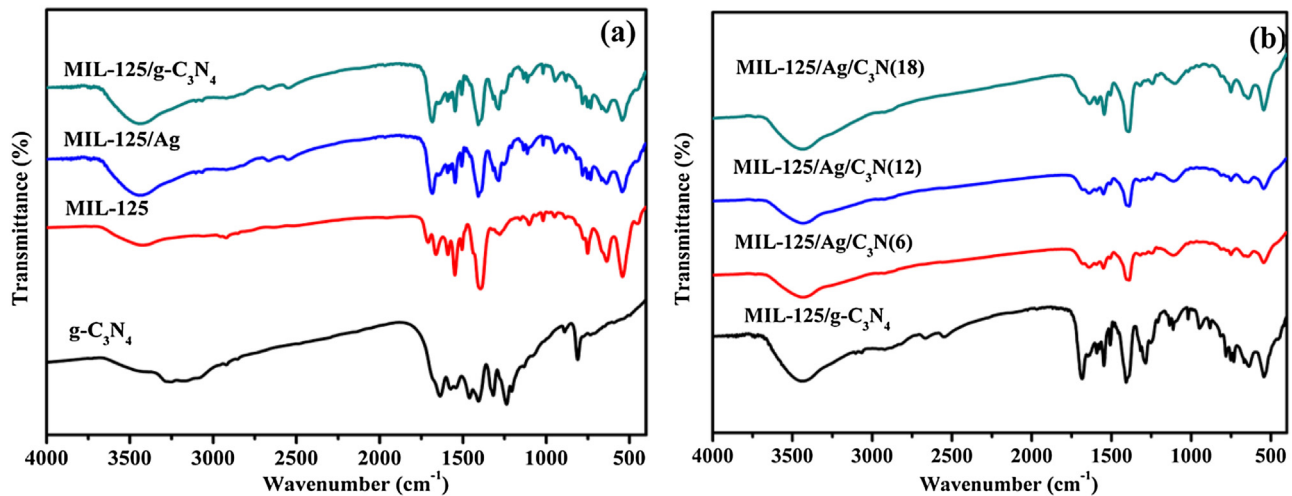


Fig. 2. FT-IR spectra of the samples.

correspond to Ag 3d<sub>3/2</sub> and Ag 3d<sub>5/2</sub> transitions, respectively. These peaks could be attributed to metallic silver (Ag<sup>0</sup>) [51].

The morphological properties of MIL-125, g-C<sub>3</sub>N<sub>4</sub> and MIL-125/Ag/g-C<sub>3</sub>N<sub>4</sub> were characterized by TEM and SEM techniques (Fig. 4). The images in Fig. 4a shows that the MIL-125 has octahedral structure shape with the size range at 300–450 nm and smooth surfaces. Fig. 4b and d shows the SEM and TEM images of g-C<sub>3</sub>N<sub>4</sub> nanosheets, and the irregular nanopieces were observed. Compared with the pure MIL-125 and g-C<sub>3</sub>N<sub>4</sub>, The surface of the MIL-125/Ag/g-C<sub>3</sub>N<sub>4</sub> particles is less smooth than the pure MIL-125 (Fig. 4c). Therefore, it is revealed that the surface of MIL-125 was encapsulated by g-C<sub>3</sub>N<sub>4</sub>. For further investigating the heterostructured MIL-125/Ag/g-C<sub>3</sub>N<sub>4</sub> microspheres, TEM characterization was performed. Fig. 4e shows the TEM image of MIL-125/Ag/g-C<sub>3</sub>N<sub>4</sub>. A two-layer composite structure was clearly observed. It can be seen that g-C<sub>3</sub>N<sub>4</sub> nanosheets is as the outer layer attached on the surface of the MIL-125, which is as the inlayer. It also reveals that black small particles of Ag NPs have been distributed on the surface of g-C<sub>3</sub>N<sub>4</sub> nanosheets and MIL-125 matrix, but a slight agglomeration can still be observed. And the selected area electron diffraction (SAED) pattern exhibited a crystalline nature of Ag (inset of Fig. 4e). These features suggest that the as-prepared MIL-125/Ag/g-C<sub>3</sub>N<sub>4</sub> microspheres have an appropriate structure for visible light pho-

tocatalysis, because the distributed Ag nanoparticles can act as a bridge to facilitate the efficient electron transportation and compress the recombination of electron-holes.

The N<sub>2</sub> adsorption-desorption isotherms on the photocatalyst samples are shown in Fig. 5a. The high specific surface area of the MIL-125 and MIL-125/Ag/g-C<sub>3</sub>N<sub>4</sub> very favorable for the heterogeneous catalysis. The Brunauer–Emmett–Telle surface area of bare MIL-125 is found to be 829.9 m<sup>2</sup> g<sup>-1</sup>, while that of MIL-125/Ag/C<sub>3</sub>N<sub>4</sub>(12) is 100.9 m<sup>2</sup> g<sup>-1</sup>, which is lower than that of pure MIL-125 due to the Ag NPs and g-C<sub>3</sub>N<sub>4</sub> were attached on the surface of MIL-125. The average pore diameter of MIL-125 is 1.20 nm, suggesting that abundant micropore is existed in MIL-125. While the average pore diameter of MIL-125/Ag/C<sub>3</sub>N<sub>4</sub>(12) is 5.69 nm, indicating the formation of mesoporous materials.

The surface adsorption of organic reactant on the catalyst was the key factor that affects the photocatalytic efficiency of heterogeneous photocatalysis. The adsorption capability of MIL-125 and MIL-125/Ag/C<sub>3</sub>N<sub>4</sub> was studied and compared with that of the bare MIL-125 are shown in Fig. 5b. It was found that the adsorption capability was decreased at all MIL-125/Ag/C<sub>3</sub>N<sub>4</sub> compounds owing to the relatively small specific surface area. The stronger adsorption capability is attributed to hydrogen bonding, *n*-π and π-π interaction between MIL-125/Ag/C<sub>3</sub>N<sub>4</sub> compounds and NB.

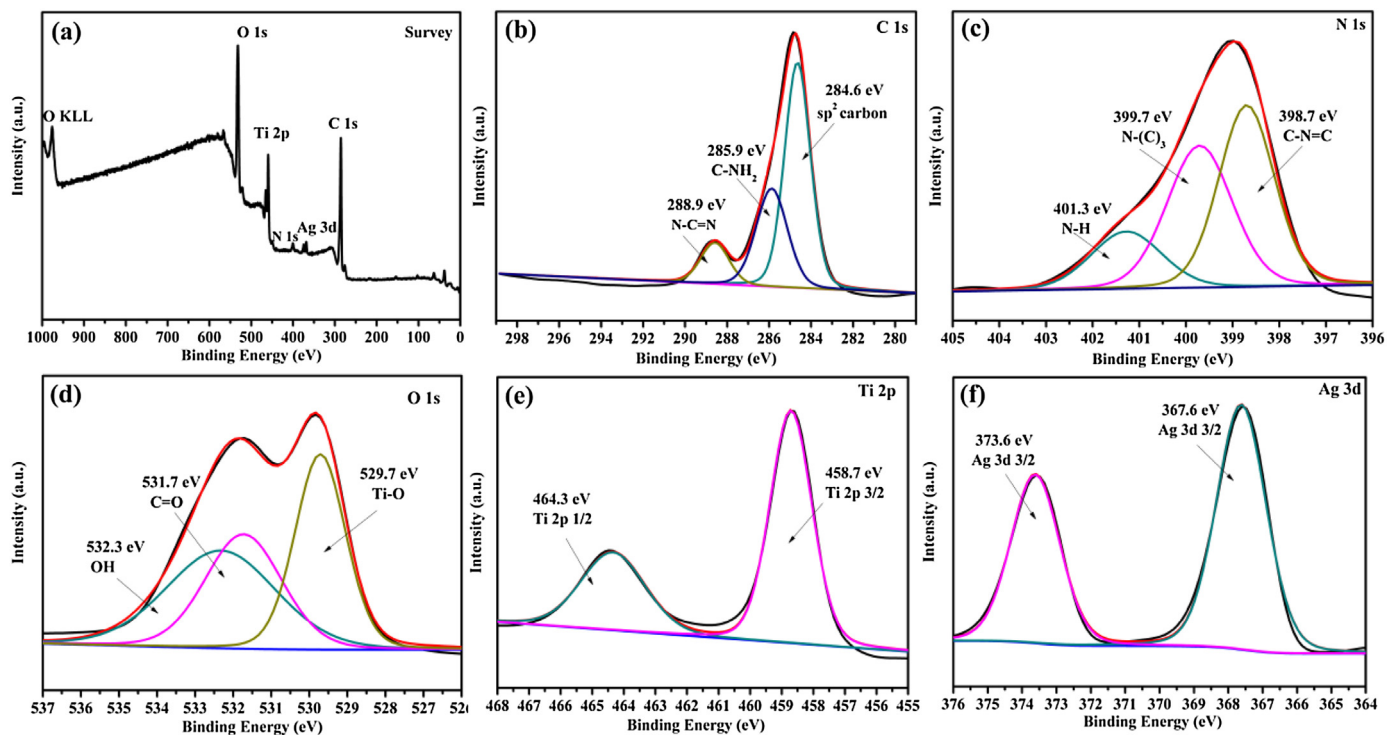


**Fig. 3.** XPS survey spectrum and the deconvoluted XPS of the MIL-125/Ag/C<sub>3</sub>N<sub>4</sub>(12). Typical wide survey (a), and high resolution XPS spectrum of C 1s (b); N 1s (c); O 1s (d); Ti 2p (e); Ag 3d (f).

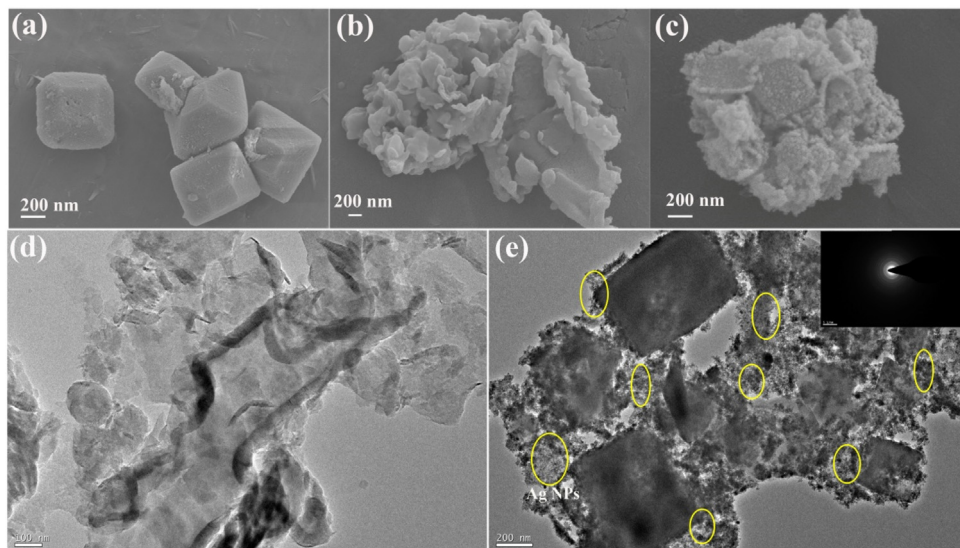


**Fig. 4.** SEM images of MIL-125 (a); C<sub>3</sub>N<sub>4</sub> nanosheets (b) and MIL-125/Ag/C<sub>3</sub>N<sub>4</sub>(12) (c); TEM of images of g-C<sub>3</sub>N<sub>4</sub> nanosheets (d) and MIL-125/Ag/C<sub>3</sub>N<sub>4</sub>(12) (e).

### 3.2. Photocatalytic activity

#### 3.2.1. Photooxidation of alcohols

The photocatalytic efficiency of the prepared MIL-125/Ag/g-C<sub>3</sub>N<sub>4</sub> nanocomposite was primarily studied by a model photooxidation reaction of benzyl alcohol. The controlled photolysis reactions (without catalysts or dark conditions) provided negligible conversion of benzyl alcohol after 6 h of irradiation time. (Table 1, Entries 1 and 5). Besides, to conform that molecular oxygen is essential for the oxidation reactions, control experiments were conducted under similar conditions but sparged with N<sub>2</sub>. The conversion was decreased obviously. More interesting, when the reaction system was carried out in the air, the benzyl alcohol obtained about 28%

conversion which is near half of that in the O<sub>2</sub> (Table 1, Entries 6, 7 and 8). The above results confirmed that the oxidation reaction is really a photocatalytic process and cannot be carried out without oxygen.

The use of MIL-125 as catalyst also provided very low conversion of benzyl alcohol, owing to its property of only UV light response (Table 1, Entry 2). Meanwhile, binary nanocomposites of MIL-125/Ag and MIL-125/g-C<sub>3</sub>N<sub>4</sub> have moderate photocatalytic activity, they can oxidize benzyl alcohol only with about 30% and 14% conversions after the same period of irradiation time, respectively (Table 1, Entries 3 and 4). It could attribute to the visible light response property of the catalysts. In contrast, using MIL-125/Ag/g-C<sub>3</sub>N<sub>4</sub> can significantly improve the conversion (up to

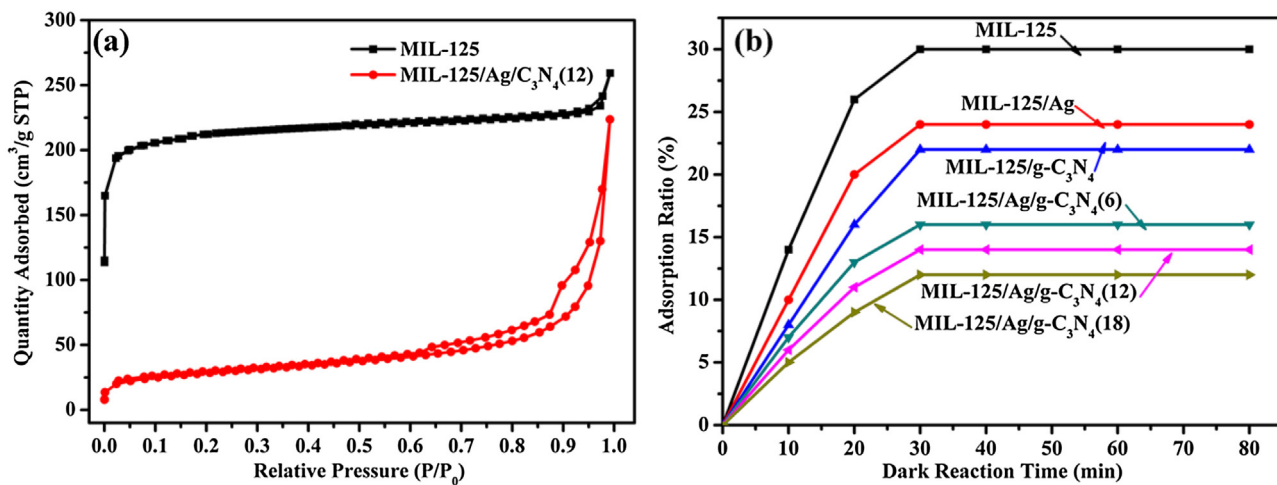


Fig. 5. N<sub>2</sub> adsorption-desorption isotherms of the samples (a) Absorption ability evaluation of the as-prepared samples for NB in dark condition (b).

**Table 1**  
Blank control experiments of the photocatalytic oxidation by MIL-125/Ag/g-C<sub>3</sub>N<sub>4</sub>.

<sup>a</sup> Entry	Catalyst	<sup>b</sup> Con. (%)	<sup>c</sup> Sel. (%)
1	none	0	0
2	MIL-125	13	93
3	MIL-125/Ag	30	98
4	MIL-125/g-C <sub>3</sub> N <sub>4</sub>	14	93
5 <sup>d</sup>	MIL-125/Ag/C <sub>3</sub> N <sub>4</sub> (12)	10	98
6 <sup>e</sup>	MIL-125/Ag/C <sub>3</sub> N <sub>4</sub> (12)	0	0
7 <sup>f</sup>	MIL-125/Ag/C <sub>3</sub> N <sub>4</sub> (12)	28	98
8	MIL-125/Ag/C <sub>3</sub> N <sub>4</sub> (12)	65	98
9	MIL-125/Ag/C <sub>3</sub> N <sub>4</sub> (18)	28	98
10	MIL-125/Ag/C <sub>3</sub> N <sub>4</sub> (6)	37	98

<sup>a</sup> Reaction conditions: 0.2 mmol substrate, 5 mg catalyst, 6 mL ethanol, O<sub>2</sub>, visible-light irradiation (>400 nm), 6 h.

<sup>b</sup> Calculated by GC analysis.

<sup>c</sup> Selectivity for aldehydes or ketones.

<sup>d</sup> In N<sub>2</sub> atmosphere.

<sup>e</sup> Without irradiation of the light.

<sup>f</sup> In the air.

65%) and with a benzaldehyde selectivity of 98% achieved under the same photocatalytic conditions. Notably, the content of g-C<sub>3</sub>N<sub>4</sub> in MIL-125/Ag/g-C<sub>3</sub>N<sub>4</sub> should be controlled at an optimal value. Photocatalytic activity of MIL-125/Ag/g-C<sub>3</sub>N<sub>4</sub> hybrids has increased along with the increase of g-C<sub>3</sub>N<sub>4</sub> content. However, when the g-C<sub>3</sub>N<sub>4</sub> nanosheets content is increased exceed 18 mL, a decrease in the photocatalytic activity was also observed. Therefore, excess g-C<sub>3</sub>N<sub>4</sub> may decrease the quality of effective heterointerfaces. It is unfavorable for the charge transfer at heterointerfaces [28]. And the results are according with the PL and EIS analysis. (Table 1, Entries 8, 9 and 10). Moreover, the selectivity of benzaldehyde was about 93% by using MIL-125 and MIL-125/g-C<sub>3</sub>N<sub>4</sub> as the catalyst. It is lower than by the MIL-125/Ag and MIL-125/Ag/g-C<sub>3</sub>N<sub>4</sub> (98%). Therefore, the structure of the catalyst also has the influence on the selectivity of the reactions.

Moreover, the photocatalytic activity of the MIL-125/Ag/g-C<sub>3</sub>N<sub>4</sub> semiconductor was examined for the oxidation of benzyl alcohol in various solvents. Catalytic results shown in Table 2 suggest that ethanol is a suitable solvent for the present photocatalytic system, giving 65% conversion of benzyl alcohol. Comparatively, other solvents, such as ethyl acetate, cyclohexane, 1,2-dichloroethane and toluene, which can all promote the photooxidation of benzyl alcohol but with significantly lower conversion yields of 30%, 40%, 38% and 28%, respectively. (Table 2, Entries 2–5). Besides, as a clear solvent, H<sub>2</sub>O also obtained a higher conversion and selectivity of 47%

**Table 2**  
Photooxidation of benzyl alcohol in different solvents.

<sup>a</sup> Entry.	Solvents	<sup>b</sup> Con. (%)	<sup>c</sup> Sel. (%)
1	Ethanol	65	98
2	Toluene	28	98
3	Ethyl acetate	30	98
4	Cyclohexane	40	97
5	1,2-Dichloroethane	38	98
6	H <sub>2</sub> O	47	97

<sup>a</sup> Reaction conditions: 0.2 mmol substrate, 5 mg catalyst, 6 mL solvents, visible-light irradiation (>400 nm), 6 h.

<sup>b</sup> Calculated by GC analysis.

<sup>c</sup> Selectivity for aldehydes or ketones.

and 97% under the unique conditions, respectively. (Table 2, Entry 6).

The MIL-125/Ag/g-C<sub>3</sub>N<sub>4</sub> is also able to photocatalyze the oxidation of various aromatic alcohols to the corresponding carbonyl compounds with sufficient conversion and selectivity. Table 3 summarizes the results obtained by the photoreaction. It can be seen that the conversion in these substrates increases proportionally with the increasing of the electron-donating ability of the corresponding substituent group in alcohols. For example, the conversions of alcohols substituted by CH<sub>3</sub>O- or CH<sub>3</sub>- were higher than that of benzyl alcohol (Table 3, Entries 1–6). On the contrary, in the case of those with an electron-withdrawing substituent, such as 4-chlorobenzyl alcohol, 4-nitrobenzyl alcohol, lower yields of the corresponding aldehyde were observed (Table 3, Entries 7 and 8). In all of the oxidations, secondary benzylic substrates give higher conversions (Entries 9–15) compared with that of the primary benzylic alcohols. Besides, the electronic effect observed from the primary benzylic systems also seems to be prevalent in the case of benzohydrol systems. For example, the existing of a chlorine group (Table 3, Entries 10 and 11) resulted in a lower conversion than that of the electron-rich ones (Table 3, Entries 12–15).

### 3.2.2. Photoreduction of nitroaromatic compounds

The photocatalytic performances of the MIL-125/Ag/g-C<sub>3</sub>N<sub>4</sub> photocatalysts were also examined by the reduction of nitrobenzene derivatives into anilines under irradiation of visible light and N<sub>2</sub> purge conditions. Fig. 6a shows the UV-vis spectra of NB aqueous solution during the photocatalytic reaction over the MIL-125 based photocatalysts in methanol for 4 h. It can be observed that a rapid decrease in the absorption of NB at 268 nm along with a simultaneous appearance of a new peak at 228 nm, which corresponds to the absorption of AN. This result indicates that photoreduc-

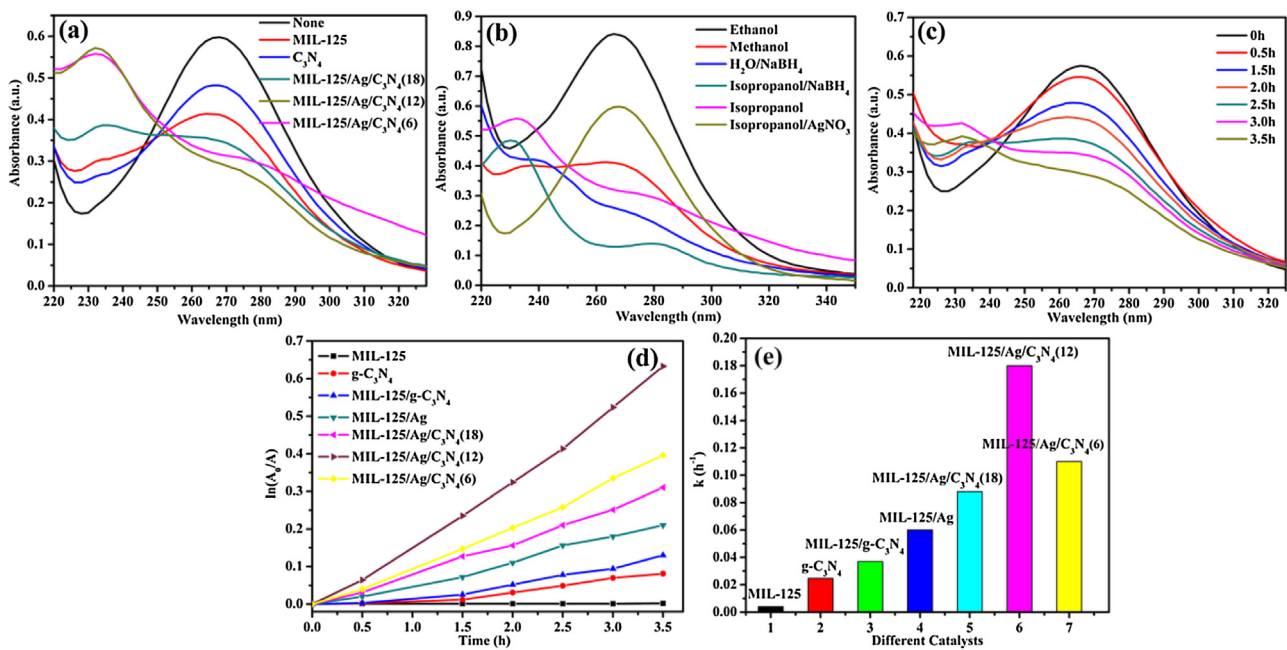


**Fig. 6.** UV-vis spectra of NB solution monitored during the photocatalytic reaction with different catalysts (a); in different solvents (b); within different reaction time catalyzed by MIL-125/Ag/C<sub>3</sub>N<sub>4</sub>(12) (c); time-online profiles of conversion of photocatalytic NB reduction over different catalysts (d) and the rate constant *k* of different catalysts (e).

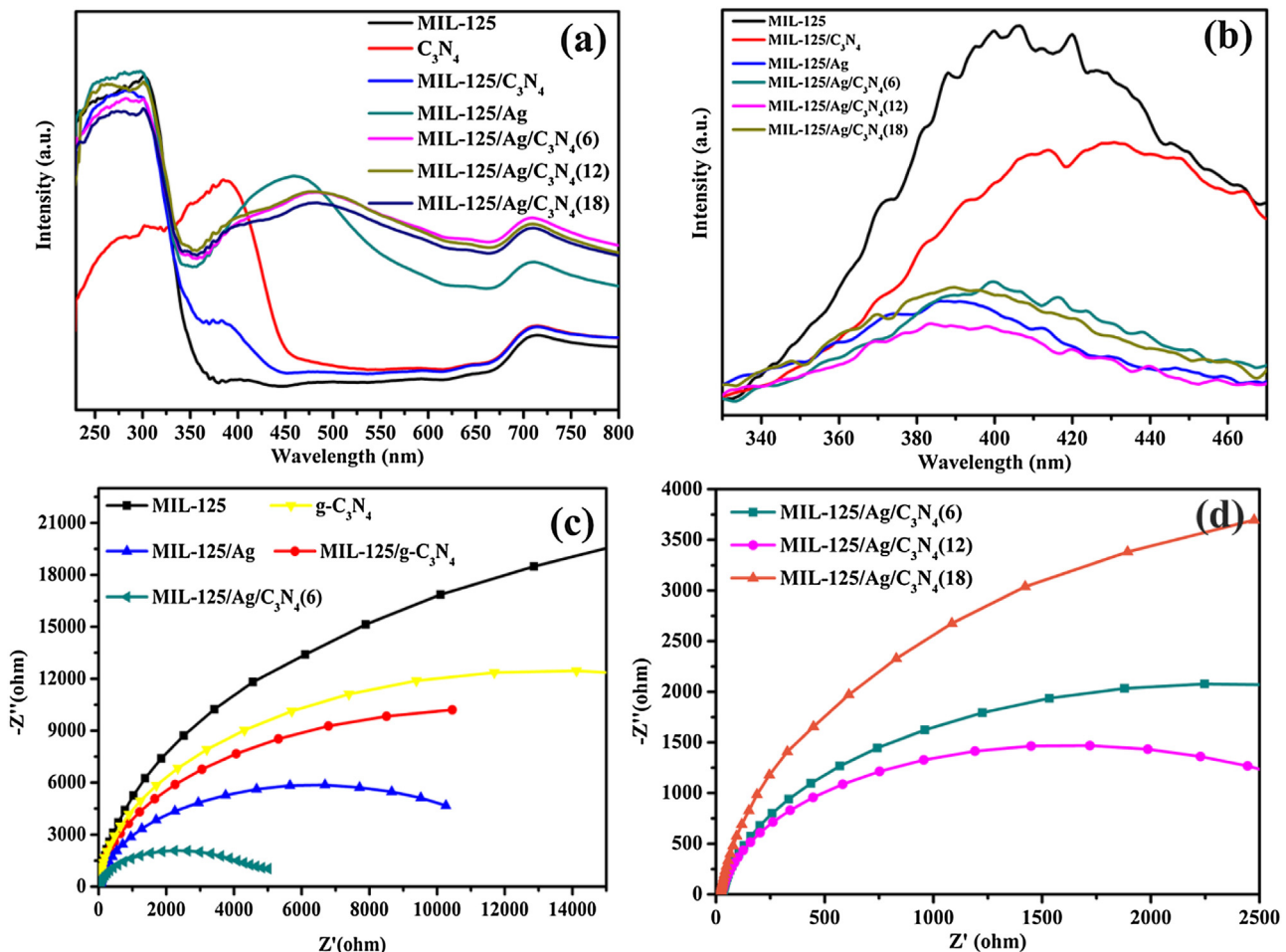


**Fig. 7.** UV-vis DRS of the samples (a); Photoluminescence spectra (PL) of the samples (b); EIS Nyquist plots of the samples under dark condition (a) and (b).

**Table 3**Photooxidation of various substituted benzyl alcohols over MIL-125/Ag/g-C<sub>3</sub>N<sub>4</sub>.

<sup>a</sup> Entry	Substrate	Product	<sup>b</sup> Con. (%)	<sup>c</sup> Sel. (%)
1			65	98
2			70	98
3			72	98
4			82	98
5			74	98
6			88	98
7			12	97
8			36	97
9			82	100
10			67	100
11			68	100
12			92	100
13			89	100
14			83	100
15			86	100

<sup>a</sup> Reaction conditions: 0.2 mmol substrate, 5 mg catalyst, 6 mL ethanol, visible-light irradiation (>400 nm), O<sub>2</sub> atmosphere; 6 h.<sup>b</sup> Conversation of the alcohols calculated by GC analysis.<sup>c</sup> Selectivity of the aldehydes or ketones.

tion of NB to AN could be achieved using MIL-125/Ag/g-C<sub>3</sub>N<sub>4</sub> nanocomposite as photocatalysts under visible light irradiation. Moreover, the photocatalytic reduction efficiency of NB follows the sequence: MIL-125/Ag/C<sub>3</sub>N<sub>4</sub>(12) > MIL-125/Ag/C<sub>3</sub>N<sub>4</sub>(6) > MIL-125/Ag/C<sub>3</sub>N<sub>4</sub>(18) > MIL-125/Ag > MIL-125/C<sub>3</sub>N<sub>4</sub> > C<sub>3</sub>N<sub>4</sub> > MIL-125. Moreover, the influence of organic solvents on the catalytic performances was also studied (Fig. 6b). It could be observed that the solvent has a great influence on the reaction. It was believed that alcohols can act as a hole scavenger, so solvent of alcohols can accelerate the photocatalytic reduction reaction and generate hydrogen proton to the reaction [52,53]. Secondary alcohol bears higher activity than the primary alcohol, so the reduction of NB has the highest activity when isopropanol was used as solvents. However, ethanol was not activated by the photoinduced holes, therefore, NB was not reduced in ethanol. In addition, the electron scavenger, AgNO<sub>3</sub> (20 mg), was added to the NB system to trap the electron [54]. The result shows that the conversion of NB decreased significantly when AgNO<sub>3</sub> was added, it is revealed that the photo-generated electrons are major active species for the reduction of the NB. We can find that NB could also be reduced

with the NaHB<sub>4</sub> as the reductant in H<sub>2</sub>O or isopropanol medium. Moreover the photoreduction of NB using MIL-125/Ag/C<sub>3</sub>N<sub>4</sub>(12) as the catalyst was performed at different time (Fig. 6c). Meanwhile, the kinetics of the reduction of NB with different catalysts was investigated. As showed in Fig. 6d, the pseudo-first-order rate law was applied for investigating the kinetics as showed in Eq. (1).

$$r = -\frac{dc}{dt} = kc = \ln \frac{C_0}{C_t} = \ln \frac{A_0}{A_t} \quad (1)$$

here *c* is the concentration of NB at various intervals, *A* is the absorbance associated to the corresponding *c*, *t* is the irradiation time (h), and *k* is the reaction rate constant (h<sup>-1</sup>). The reaction rate constants (*k*) is obtained for herbicide degradation from plotting the graph of ln(*A*<sub>0</sub>/*A*<sub>t</sub>) versus *t*.

Moreover, the values of *k* are shown in Fig. 6e. The order of photoreduction of NB rate for as prepared photocatalysts is MIL-125/Ag/C<sub>3</sub>N<sub>4</sub>(12) (0.18 h<sup>-1</sup>) > MIL-125/Ag/C<sub>3</sub>N<sub>4</sub>(6) (0.11 h<sup>-1</sup>) > MIL-125/Ag/C<sub>3</sub>N<sub>4</sub>(18) (0.088 h<sup>-1</sup>) > MIL-125/Ag (0.061 h<sup>-1</sup>) > MIL-125/C<sub>3</sub>N<sub>4</sub> (0.037 h<sup>-1</sup>) > C<sub>3</sub>N<sub>4</sub> (0.025 h<sup>-1</sup>) > MIL-125 (0.004 h<sup>-1</sup>). It is more directly demonstrated that

MIL-125/Ag/C<sub>3</sub>N<sub>4</sub> (12) has the highest photocatalytic activity. The result is similar to the above result of Fig. 6a and the photooxidation of benzyl alcohol.

As shown in Table 4, photocatalytic reduction of various aromatic nitro compounds, including electron-rich and electron-deficient substrates, was proceeded readily at simple experimental condition to afford well to excellent conversion of the corresponding amines. It can be seen that the chemical activity of the substrates depends strongly on the electron withdrawing or electron donating nature of the functional groups on the aromatic rings. For example, nitro compounds with electron withdrawing groups (such as –Cl, –NO<sub>2</sub>, –COR and –C<sub>6</sub>H<sub>5</sub>) have higher reaction activity (Table 4, Entries 2–5, 12 and 13) than those with electron donating substituents (e.g. –CH<sub>3</sub>, –OCH<sub>3</sub>) (Table 4, Entries 9–11, 15), because they have obtained the similar conversion with a shorter time. It also shown that during the photocatalytic reduction of the nitro compounds, the carbonyl group present in the aromatic ring remained unaffected (Table 4, Entry 15). The aromatic nitro compounds including –OH, an electron donating group, bears higher activity, the possible reason is attributed to the acidity of phenol. That is, nitrophenol has the strong acidity than NB, it could be beneficial to the photoreduction.

### 3.3. Photocatalytic mechanism

The optical absorption properties of the as-prepared samples were investigated using UV-vis spectrophotometry. As shown in Fig. 7a, pure C<sub>3</sub>N<sub>4</sub> nanosheets absorb the light from the ultraviolet to visible-light field, and its band gap absorption edge is around 470 nm. While no obvious absorption peak in the visible area is detected for MIL-125 indicating that it does not possess the ability to utilize photo-energy in the visible-light range. The absorption edge of MIL-125 is about 345 nm, originated from its band gap, the value of Eg is about 3.6 eV, in good accordance with the reported results [41]. For the MIL-125/C<sub>3</sub>N<sub>4</sub> composite, the absorption edges with a slight red-shift were displayed. Moreover, a notable absorption extension in the visible light region could be observed in the MIL-125/Ag composite, it is due to the strong absorption in the visible light range of Ag NPs [55]. For the MIL-125/Ag/g-C<sub>3</sub>N<sub>4</sub> nanocomposites, the similar absorption extension in the visible-light region was presented. Moreover, attributed to the integrative effect of the enhanced light absorption intensity by the C<sub>3</sub>N<sub>4</sub> nanosheets and Ag NPs, they have the largest absorption edges compared with that of MIL-125, MIL-125/C<sub>3</sub>N<sub>4</sub> and MIL-125/Ag, suggesting their potential capability of effectively utilizing of visible-light energy.

The recombination of electron-hole pairs can release energy, which can be also detected by PL emission. A lower PL intensity is a general indication of a lower recombination of electron-hole pairs, resulting in higher photocatalytic activity [56]. The PL spectra of the samples were presented in Fig. 7b. MIL-125 has a strong PL emission peak at around 400 nm. It is attributed to the H<sub>2</sub>BDC ligand [57]. In comparison with MIL-125, the peaks intensities of MIL-125/C<sub>3</sub>N<sub>4</sub>, MIL-125/Ag and MIL-125/Ag/g-C<sub>3</sub>N<sub>4</sub> are much lower. It is showed that the recombination inhibition of electrons and holes in MIL-125/C<sub>3</sub>N<sub>4</sub>, MIL-125/Ag and MIL-125/Ag/g-C<sub>3</sub>N<sub>4</sub> are more efficient than that of the pure MIL-125. Especially, MIL-125/Ag/C<sub>3</sub>N<sub>4</sub>(12) has the lowest emission peak at the position of 400 nm, suggesting the lowest recombination rate of photoinduced electron-hole pairs. So the reason of highest photocatalytic activity and conversion of benzyl alcohol and nitrobenzene obtained by MIL-125/Ag/C<sub>3</sub>N<sub>4</sub>(12) would be attributed to its lowest recombination of electron-hole pairs. The highest photocatalytic activity of MIL-125/Ag/C<sub>3</sub>N<sub>4</sub>(12) was consistent with its highest charge-separation efficiency.

Electrochemical impedance spectroscopy (EIS) measurements were carried out to study the interface charge transport behavior

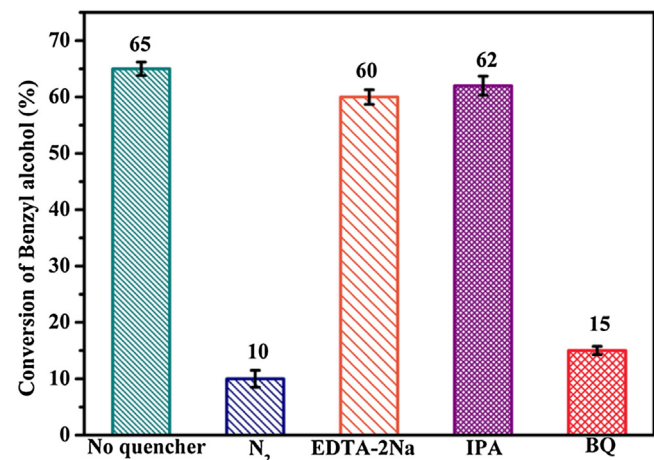


Fig. 8. Effects of different reactive species scavengers on the photocatalytic oxidation of benzyl alcohol by MIL-125/Ag/C<sub>3</sub>N<sub>4</sub>(12) under visible-light irradiation.

in the hybrid system. Fig. 7c shows the EIS responses of MIL-125, g-C<sub>3</sub>N<sub>4</sub>, MIL-125/Ag, MIL-125/C<sub>3</sub>N<sub>4</sub> and MIL-125/Ag/g-C<sub>3</sub>N<sub>4</sub>(6). The radius of the arc on the EIS Nyquist plot reflects the reaction rate occurring at the electrode surface. The decrease of the arc radius indicates a fast interfacial charge transfer and an effective separation of the photogenerated electron-hole pairs occurred in the hybrid [58,59]. These electrodes show a pronounced arc (semicircle portion) at higher frequencies in the EIS plane. Clearly, a smaller arc radius was observed for the MIL-125/Ag/g-C<sub>3</sub>N<sub>4</sub> composite as compared to those of MIL-125, g-C<sub>3</sub>N<sub>4</sub>, MIL-125/Ag and MIL-125/C<sub>3</sub>N<sub>4</sub>. These results clearly show that the incorporation of MIL-125, Ag and g-C<sub>3</sub>N<sub>4</sub> remarkably enhance the electron mobility by reducing the recombination of electron-hole pairs, which is in accordance with its higher photocatalytic reactivity for the oxidation of benzyl alcohol and the reduction of nitro compounds. For the MIL-125/Ag/g-C<sub>3</sub>N<sub>4</sub> composite with different content of g-C<sub>3</sub>N<sub>4</sub> nanosheets, it is obviously observed that MIL-125/Ag/C<sub>3</sub>N<sub>4</sub>(12) has the smallest reduction of arc radius than that of MIL-125/Ag/C<sub>3</sub>N<sub>4</sub>(6) and MIL-125/Ag/C<sub>3</sub>N<sub>4</sub>(18), indicating that the MIL-125/Ag/C<sub>3</sub>N<sub>4</sub>(12) has the lowest recombination of electron-hole pairs (Fig. 7d).

To evaluate the mechanism for the photooxidation of the benzyl alcohol, main oxidative species in the photocatalytic process were detected through radical and hole trapping experiments using EDTA-2Na (scavenger of h<sup>+</sup>), p-benzoquinone (BQ, scavenger of •O<sub>2</sub><sup>–</sup>), isopropyl alcohol (scavenger of •OH), or N<sub>2</sub> flow (excluding O<sub>2</sub>) [28,60,61]. As depicted in Fig. 8, ignorable decrease is shown by isopropyl alcohol, implying the absence of •OH species. Besides, most of the reaction system are water-free, there is little opportunity to achieve the transform H<sub>2</sub>O into •OH. Moreover, the photo-induced holes of g-C<sub>3</sub>N<sub>4</sub> cannot oxidize the adsorbed H<sub>2</sub>O molecules to •OH, because the value band potential of g-C<sub>3</sub>N<sub>4</sub> (+1.6 eV vs. NHE) is less positive than the standard redox potential E<sup>0</sup>(•OH/H<sub>2</sub>O) (+2.8 eV vs. NHE). The conversion of benzyl alcohol also decreased slightly in the presence of 1 mmol EDTA-2Na, indicating few of h<sup>+</sup> takes part in the oxidation of the benzyl alcohol. As the previous study of us, the benzyl alcohol could be oxidized by h<sup>+</sup> directly when the value band potential of semiconductor is located in the 1.88 ~ 2.27 eV [62], therefore, the holes of g-C<sub>3</sub>N<sub>4</sub> cannot oxidize the benzyl alcohol into benzaldehyde.

The conversion of the benzyl alcohol obviously decreased from 65% to 15% in the presence of 1 mmol BQ, suggesting the active species of •O<sub>2</sub><sup>–</sup> played an important role. To further confirm the point, the reaction was carried out in the N<sub>2</sub> atmosphere, the conversion of the benzyl alcohol was enormously decreased by the

**Table 4**Photoreduction of various nitrobenzene derivatives over MIL-125/Ag/g-C<sub>3</sub>N<sub>4</sub>.

<sup>a</sup> Entry	Substrate	Product	Time (h)	<sup>b</sup> Conv. (%)	<sup>c</sup> Sel. (%)
1			4	74	98
2.			1.5	78	98
3			1.5	80	99
4			1.5	80	99
5			2	86	99
6			0.5	82	99
7			0.5	80	99
8			0.5	82	99
9			5	77	99
10			5	75	99
11			5	75	99
12			2	83	99
13			0.5	82	99
14			1.5	82	96
15			2	82	97

<sup>a</sup> Reaction conditions: 0.1 mmol substrate, 5 mg catalyst, 6 mL isopropyl alcohol, visible-light irradiation (>400 nm), N<sub>2</sub> atmosphere.<sup>b</sup> Conversation of the nitrocompound calculated by GC analysis.<sup>c</sup> Selectivity of the aromatic amine.

conducted N<sub>2</sub> (no scavenger), which decreased from conversion 65% under aerobic conditions to 10% under N<sub>2</sub> atmosphere. The result has demonstrated that the dissolved oxygen which could act as a photo-generated electron scavenger to produce •O<sub>2</sub><sup>−</sup> radical species. As a result, it could be preliminarily concluded that •O<sub>2</sub><sup>−</sup> generated in the photocatalytic system should be responsible for the enhanced photooxidation performance towards benzyl alcohol.

For the photocatalytic reduction of nitrobenzene, firstly, the N<sub>2</sub> purge condition provides an anaerobic atmosphere for the reaction. Thus, the nitrobenzene has no opportunity to undergo the oxidation reaction. The photogenerated holes are quenched by the solvent of alcohols, which results in a producing of the active protons [63]. At the same time, nitrobenzene captures the active proton and the photoexcited electrons generated by visual light irradiation, and then aniline formed. In the above-mentioned experimental result, it is also revealed that the photo-generated electrons are major active species for the reduction of the NB. It is clear that the photogenerated holes and photogenerated electrons should play the same crucial roles in the reduction nitrobenzene process.

On the basis of these results, we suggest a possible reaction mechanism for the present photocatalytic system. As shown in **Scheme 2**, under visible-light irradiation, both g-C<sub>3</sub>N<sub>4</sub> and Ag NPs could absorb the visible light and be excited to the generation of electrons (e<sup>−</sup>) and holes (h<sup>+</sup>). The joint UV-vis DRS, PL and EIS characterization faithfully demonstrate that metallic Ag played an

important role for the in two aspects. On one hand, as an electron donor, Ag nanoparticles could absorb the incident photons and produced electrons and holes attributable to the surface plasmon resonance (SPR) by the induced electronic field [31,34,60]. On the other hand, Ag NPs deposited on the surface of MIL-125 played an important role as an electron-conduction bridge. The electrons transfer toward MIL-125 and the electron-holes separation in g-C<sub>3</sub>N<sub>4</sub> would be more efficient because of the formed Schottky barrier at the interface of Ag NPs and MIL-125 [64,65]. Besides, the photoinduced electrons from g-C<sub>3</sub>N<sub>4</sub> directionally migrate to MIL-125 due to the close interfacial connections between MIL-125, Ag NPs and g-C<sub>3</sub>N<sub>4</sub>, where photoinduced electrons and holes are efficiently separated in space, which is conducive to retarding the recombination of electron-holes and improving the photoactivity [66]. Therefore, the photoinduced electrons on g-C<sub>3</sub>N<sub>4</sub> and Ag NPs can transfer easily to the Ti<sup>4+</sup> species in the titanium-oxo cluster of MIL-125(Ti) via the heterojunctional structure, resulting in the reduction of Ti<sup>4+</sup> to Ti<sup>3+</sup> [67,68].

For the photooxidation of the benzyl alcohol, oxygen molecules adsorbed onto porous MIL-125(Ti) form superoxide (•O<sub>2</sub><sup>−</sup>) ion radicals via electron transfer from Ti<sup>3+</sup> to O<sub>2</sub> molecules due to the strong reducing ability of Ti<sup>3+</sup> (-1.37 V vs. SHE). Then the Ti<sup>3+</sup> ions are oxidized and further convert to Ti<sup>4+</sup> ions [17,69,70]. The formed •O<sub>2</sub><sup>−</sup> radicals could efficiently oxidize benzyl alcohol into benzaldehyde. Simultaneously, the generated holes of g-C<sub>3</sub>N<sub>4</sub> and Ag NPs

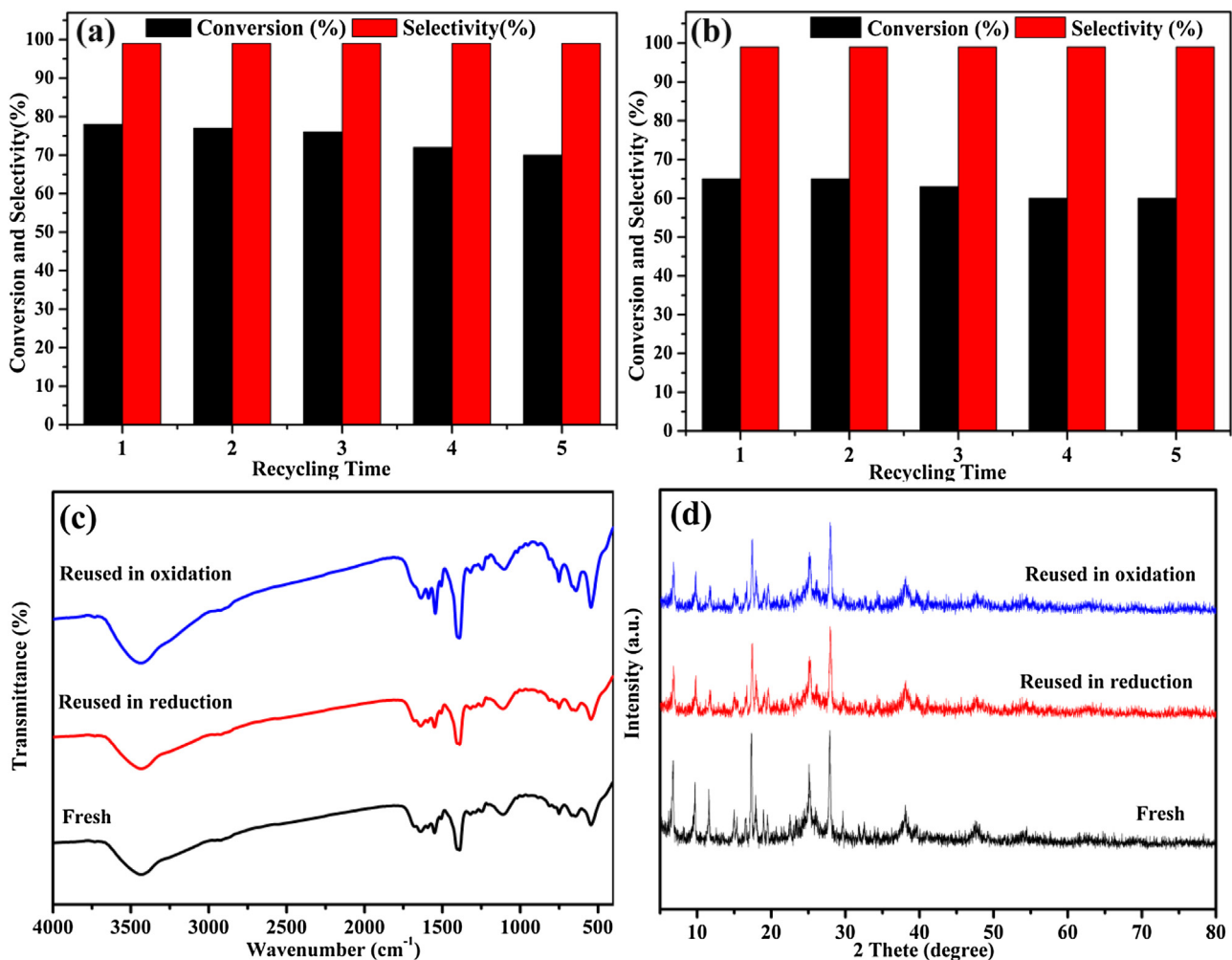


**Fig. 9.** The cycling runs at the oxidation of the benzyl alcohol over MIL-125/Ag/g-C<sub>3</sub>N<sub>4</sub>(12) system (a); the reduction of nitrobenzene(b); the FT-IR spectra (c) and PXRD patterns (d) of MIL-125/Ag/g-C<sub>3</sub>N<sub>4</sub>(12) before and after the catalytic reactions.

can induce the oxidation of alcohols to producing the corresponding cationic radicals, which will succulently react with  $\bullet\text{O}_2^-$  to form the corresponding carbonyl compounds [71]. For the photocatalytic reduction of nitrobenzene, the photogenerated holes by g-C<sub>3</sub>N<sub>4</sub> and Ag NPs are quenched by the solvent of alcohols and producing the active protons. The photoinduced electrons and active protons could be further captured by NB, finally AN was formed.

#### 3.4. Recyclability and stability of the catalyst

The stability of MIL-125/Ag/g-C<sub>3</sub>N<sub>4</sub> nanocomposite was tested through the reduction of nitrobenzene and the oxidation of benzyl alcohol, respectively. After the reactions, the catalyst was centrifugalized and washed with deionized water then the recovered catalyst was dried at 60 °C for 12 h and used for the next run. As shown in Fig. 9a and 9b, the cyclic experimental results for the reduction and the oxidation demonstrated that after 4 times of recycling, the conversions were still maintained between 70% and 60%, respectively. There is no significant decrease found. It indicates that the photocatalytic activity of MIL-125/Ag/g-C<sub>3</sub>N<sub>4</sub> was well maintained. It is supposed that the little mass loss in the progress of recovery is the main reason which caused the slight decreases in photocatalytic activity of reused photocatalyst in the five repeat. The structural stability of MIL-125/Ag/g-C<sub>3</sub>N<sub>4</sub> was further investigated by FT-IR and XRD methods of the fresh and the four-cycled samples. As shown in Fig. 9c and 9d, both of the FT-IR

spectra and the XRD patterns of the fresh and the used samples showed no obvious difference. Besides, the (111) plane of Ag NPs was also remained, indicating that the structure and contents of Ag NPs were not changed. So it revealed that the structure of MIL-125/Ag/g-C<sub>3</sub>N<sub>4</sub> was well maintained even after a four cycles in the reaction. Therefore, it can be concluded that the photocatalyst bears good recyclability under the experimental conditions.

#### 4. Conclusions

In summary, heterostructured MIL-125/Ag/g-C<sub>3</sub>N<sub>4</sub> nanocomposite was successfully constructed via an accessible photo-deposition and mild chemical process. During this process, MIL-125/Ag was firstly synthesized by a photo-reduction deposition method, followed by the adhering of g-C<sub>3</sub>N<sub>4</sub> onto the MIL-125/Ag composite. It was found that MIL-125/Ag/g-C<sub>3</sub>N<sub>4</sub> nanocomposite is an efficient visible-light response photocatalyst for the photoreduction of nitrocompounds and the photooxidation of alcohols. The photoreduction and photooxidation results together with the PL and EIS analysis revealed that the mass ratio of g-C<sub>3</sub>N<sub>4</sub> in MIL-125/Ag/g-C<sub>3</sub>N<sub>4</sub> showed a significant effect on the separation of photogenerated charge carriers as well as the visible light photocatalytic activity. The MIL-125/Ag/g-C<sub>3</sub>N<sub>4</sub>(12) sample showed the significantly enhanced photocatalytic activity as compared with the bare MIL-125, g-C<sub>3</sub>N<sub>4</sub>, MIL-125/Ag and MIL-125/C<sub>3</sub>N<sub>4</sub>. Moreover, it is also proved that Ag NPs was uni-

formly photodeposited on the surface of g-C<sub>3</sub>N<sub>4</sub> and MIL-125, which can not only increase the visible-light absorption via the surface plasmon resonance but also play an important role as an electron-conduction bridge between MIL-125/Ag and g-C<sub>3</sub>N<sub>4</sub>. Therefore, the photocatalytic activity of the natural MIL-125 is effectively improved. Furthermore, the MIL-125/Ag/g-C<sub>3</sub>N<sub>4</sub> sample exhibited good recyclability under visible-light irradiation. On the basis of the above results of this study, the MIL-125/Ag/g-C<sub>3</sub>N<sub>4</sub> nanocomposite is expected to be effective as a useful visible-light photocatalyst for organic transformation, it provides an economical, sustainable and green process for the synthesis of amine and aldehydes. The research highlights the great potential of MOFs as photocatalysts for many organic syntheses.

## Acknowledgements

The research was financial supported by NSFC(21563026, 21163016), Gansu provincial Natural Science Foundation of China (1208RJZA287), and the Program for Changjiang Scholars and Innovative Research Team in University (IRT15R56). We also thank the Key Laboratory of Eco-Environment-Related Polymer Materials (Northwest Normal University), Ministry of Education, for financial support.

## References

- [1] N. Stock, S. Biswas, *Chem. Rev.* 112 (2011) 933–969.
- [2] S. Proch, J. Herrmannsdorfer, R. Kempe, C. Kern, A. Jess, L. Seyfarth, J. Senker, *Chem. Eur. J.* 14 (2008) 8204–8212.
- [3] E. López Maya, C. Montoro, V. Colombo, E. Barea, J.A. Navarro, *Adv. Funct. Mater.* 24 (2014) 6130–6135.
- [4] M. Zhao, S. Ou, C.D. Wu, *Acc. Chem. Res.* 47 (2014) 1199–1207.
- [5] P. Wu, J. Wang, Y. Li, C. He, Z. Xie, C. Duan, *Adv. Funct. Mater.* 21 (2011) 2788–2794.
- [6] K.E. Wang, W. deKrafft, W. Lin, *J. Am. Chem. Soc.* 134 (2012) 7211–7214.
- [7] Q. Li, N. Zhang, Y. Yang, G. Wang, D.H. Ng, *Langmuir* 30 (2014) 8965–8972.
- [8] L. Shi, T. Wang, H. Zhang, K. Chang, J. Ye, *Adv. Funct. Mater.* 25 (2015) 5360–5367.
- [9] R. Liang, L. Shen, F. Jing, N. Qin, L. Wu, *ACS Appl. Mater. Inter.* 7 (2015) 9507–9515.
- [10] L. Shi, T. Wang, H. Zhang, K. Chang, X. Meng, H. Liu, J. Ye, *Adv. Sci.* 2 (2015).
- [11] R. Liang, S. Luo, F. Jing, L. Shen, N. Qin, L. Wu, *Appl. Catal. B: Environ.* 176–177 (2015) 240–248.
- [12] Y. Fu, D. Sun, Y. Chen, R. Huang, Z. Ding, X. Fu, Z. Li, *Angew. Chem. Int. Ed.* 51 (2012) 3364–3367.
- [13] S. Abedi, A. Morsali, *ACS Catal.* 4 (2014) 1398–1403.
- [14] M. Nasalevich, R. Becker, E. Ramos-Fernandez, S. Castellanos, S.L. Veber, M.V. Fedin, F. Kapteijn, J. Reek, J.I. van der Vlugt, J. Gascon, *Energy Environ. Sci.* 8 (2015) 364–375.
- [15] C.H. Hendon, D. Tiana, M. Fontecave, C.m. Sanchez, L. D'arras, C. Sasso, L. Rozes, C. Mellot Draznieks, A. Walsh, *J. Am. Chem. Soc.* 135 (2013) 10942–10945.
- [16] D. Sun, W. Liu, Y. Fu, Z. Fang, F. Sun, X. Fu, Y. Zhang, Z. Li, *Chem. Eur. J.* 20 (2014) 4780–4788.
- [17] H. Wang, X. Yuan, Y. Wu, G. Zeng, H. Dong, X. Chen, L. Leng, Z. Wu, L. Peng, *Appl. Catal. B: Environ.* 186 (2016) 19–29.
- [18] Y. Fu, L. Sun, H. Yang, L. Xu, F. Zhang, W. Zhu, *Appl. Catal. B: Environ.* 187 (2016) 212–217.
- [19] J. He, Z. Yan, J. Wang, J. Xie, L. Jiang, Y. Shi, F. Yuan, F. Yu, Y. Sun, *Chem. Commun.* 49 (2013) 6761–6763.
- [20] C.F. Zhang, L.G. Qiu, F. Ke, Y.J. Zhu, Y.P. Yuan, G.S. Xu, X. Jiang, *J. Am. Chem. Soc.* 1 (2013) 14329–14334.
- [21] R. Wang, L. Gu, J. Zhou, X. Liu, F. Teng, C. Li, Y. Shen, Y. Yuan, *Adv. Mater. Inter.* 2 (2015).
- [22] W. Zhu, P. Liu, S. Xiao, W. Wang, D. Zhang, H. Li, *Appl. Catal. B: Environ.* 172–173 (2015) 46–51.
- [23] Y. Zheng, J. Liu, J. Liang, M. Jaroniec, S.Z. Qiao, *Energy Environ. Sci.* 5 (2012) 6717–6731.
- [24] X. Chen, Q. Liu, Q. Wu, P. Du, J. Zhu, S. Dai, S. Yang, *Adv. Funct. Mater.* 11 (2016).
- [25] S. Cao, J. Yu, *J. Phys. Chem. Lett.* 5 (2014) 2101–2107.
- [26] J. Liu, Y. Yang, N. Liu, Y. Liu, H. Huang, Z. Kang, *Green Chem.* 16 (2014) 4559–4565.
- [27] S. Ye, R. Wang, M.Z. Wu, Y.P. Yuan, *Appl. Sur. Sci.* 358 (2015) 15–27.
- [28] H. Wang, X. Yuan, Y. Wu, G. Zeng, X. Chen, L. Leng, H. Li, *Appl. Catal. B: Environ.* 174–175 (2015) 445–454.
- [29] Y.P. Zhu, M. Li, Y.L. Liu, T.Z. Ren, Z.Y. Yuan, *J. Phys. Chem. C* 118 (2014) 10963–10971.
- [30] J. Jiang, X. Zhang, P. Sun, L. Zhang, *J. Phys. Chem. C* 115 (2011) 20555–20564.
- [31] C. Yu, L. Wei, X. Li, J. Chen, Q. Fan, J.C. Yu, *Mat Sci. Eng. B Solid* 178 (2013) 344–348.
- [32] Z. Liu, Y. Huang, Q. Xiao, H. Zhu, *Green Chem.* 18 (2016) 817–825.
- [33] S. Zhang, J. Li, X. Wang, Y. Huang, M. Zeng, J. Xu, *ACS Appl. Mater. Inter.* 6 (2014) 22116–22125.
- [34] M. Hosseini Sarvari, T. Ataee Kachouei, F. Moeini, *Mater. Res. Bull.* 72 (2015) 98–105.
- [35] L. Pan, M.Y. Xu, L.J. Feng, Q. Chen, Y.J. He, B.H. Han, *Polym. Chem.* 7 (2016) 2299–2307.
- [36] C. Wang, Z. Lu, *Org. Chem. Front.* 2 (2015) 179–190.
- [37] T. Toyao, M. Saito, Y. Horiuchi, K. Mochizuki, M. Iwata, H. Higashimura, M. Matsuoka, *Cataly. Sci. Technol.* 3 (2013) 2092–2097.
- [38] R.M. Mohamed, F.M. Ibrahim, *J. Ind. Eng. Chem.* 22 (2015) 28–33.
- [39] W.C. Peng, Y. Chen, X.Y. Li, *J. Hazard. Mater.* 309 (2016) 173–179.
- [40] S. Farhadi, A. Zabardasti, Z. Babazadeh, *Tetrahedron Lett.* 47 (2006) 8953–8957.
- [41] C.H. Hendon, D. Tiana, M. Fontecave, C. Sanchez, L. D'arras, C. Sasso, L. Rozes, C. Mellot Draznieks, A. Walsh, *J. Am. Chem. Soc.* 135 (2013) 10942–10945.
- [42] X. Zhang, X. Xie, H. Wang, J. Zhang, B. Pan, Y. Xie, *J. Am. Chem. Soc.* 135 (2012) 18–21.
- [43] M. Dan Hardi, C. Serre, T. Frot, L. Rozes, G. Maurin, C. Sanchez, G. Férey, *J. Am. Chem. Soc.* 131 (31) (2009) 10857–10859.
- [44] J.C. Wang, H.C. Yao, Z.Y. Fan, L. Zhang, J.S. Wang, S.Q. Zang, Z.J. Li, *ACS Appl. Mater. Inter.* 8 (2016) 3765–3775.
- [45] M.J. Height, S.E. Pratsinis, O. Mekasuwandumrong, P. Praserttham, *Appl. Catal. B: Environ.* 63 (2006) 305–312.
- [46] S.N. Kim, J. Kim, H.Y. Kim, H.Y. Cho, W.S. Ahn, *Catal. Today* 204 (2013) 85–93.
- [47] M. Xu, L. Han, S. Dong, *ACS Appl. Mater. Inter.* 5 (2013) 12533–12540.
- [48] N. Boonprakob, N. Wetchakun, S. Phanichphant, D. Waxler, P. Sherrell, A. Nattestad, J. Chen, B. Inceesungvorn, *J. Colloid. Inter. Sci.* 417 (2014) 402–409.
- [49] J. Yan, Z. Chen, H. Ji, Z. Liu, X. Wang, Y. Xu, X. She, L. Huang, L. Xu, H. Xu, H. Li, *Chem. Eur. J.* 22 (2016) 4764–4773.
- [50] H. Guo, D. Guo, Z. Zheng, W. Weng, J. Chen, *Appl. Organomet. Chem.* 29 (2015) 618–623.
- [51] T. Potlog, D. Duca, M. Dobromir, *Appl. Sur. Sci.* 352 (2015) 33–37.
- [52] C. Liu, J.Y. Liang, R.R. Han, Y.Z. Wang, J. Zhao, Q.J. Huang, J. Chen, W.H. Hou, *Phys. Chem. Chem. Phys.* 17 (2015) 15165–15172.
- [53] W.T. Chen, A. Chan, Z.H. Al Azri, A.G. Dosado, M.A. Nadeem, D. Sun Waterhouse, H. Idriss, G.I. Waterhouse, *J. Catal.* 329 (2015) 499–513.
- [54] R. Bera, S. Kundu, A. Patra, *ACS Appl. Mater. Inter.* 7 (2015) 13251–13259.
- [55] (a) T. Liu, B. Li, Y. Wang, Z. Ge, J. Shi, *Asian J. Chem.* 26 (2014) 1355–1362; (b) Y. Hou, F. Zuo, A.P. Dagg, J. Liu, P. Feng, *Adv. Mater.* 26 (2014) 5043–5049.
- [56] X. Zhou, B. Jin, L. Li, F. Peng, H. Wang, H. Yu, Y. Fang, *J. Mater. Chem. A* 22 (2012) 17900–17905.
- [57] D. Sun, Y. Fu, W. Liu, L. Ye, D. Wang, L. Yang, X. Fu, Z. Li, *Chem. Eur. J.* 19 (2013) 14279–14285.
- [58] Y. Hou, F. Zuo, A.P. Dagg, J. Liu, P. Feng, *Adv. Mater.* 26 (2014) 5043–5049.
- [59] X. Bai, L. Wang, R. Zong, Y. Zhu, *J. Phys. Chem. C* 117 (2013) 9952–9961.
- [60] F. Chen, Q. Yang, Y. Zhong, H. An, J. Zhao, T. Xie, Q. Xu, X. Li, D. Wang, G. Zeng, *Water Res.* 101 (2016) 555–563.
- [61] F. Chen, Q. Yang, X. Li, G. Zeng, D. Wang, C. Niu, J. Zhao, H. An, T. Xie, Y. Deng, *Appl. Catal. B: Environ.* 200 (2017) 330–342.
- [62] Z. Yang, X. Xu, X. Liang, C. Lei, Y. Wei, P. He, B. Lv, H. Ma, Z. Lei, *Appl. Catal. B: Environ.* 198 (2016) 112–123.
- [63] X. Ning, S. Meng, X. Fu, X. Ye, S. Chen, *Green Chem.* (2016).
- [64] L. Shen, M. Luo, L. Huang, P. Feng, L. Wu, *Inorg. Chem.* 54 (2015) 1191–1193.
- [65] J. Chen, J. Cen, X. Xu, X. Li, *Cataly. Sci. Technol.* 6 (2) (2016) 349–362.
- [66] Y. Chen, W. Huang, D. He, Y. Situ, H. Huang, *ACS Appl. Mater. Inter.* 6 (2014) 14405–14414.
- [67] Y. Fu, D. Sun, Y. Chen, R. Huang, Z. Ding, X. Fu, Z. Li, *Angew. Chem. Int. Ed.* 124 (2012) 3420–3423.
- [68] H. Wang, X. Yuan, Y. Wu, G. Zeng, X. Chen, L. Leng, Z. Wu, L. Jiang, H. Li, *J. Hazard. Mater.* 286 (2015) 187–194.
- [69] A. Li, T. Wang, X. Chang, W. Cai, P. Zhang, J. Zhang, J. Gong, *Chem. Sci.* 7 (2) (2016) 890–895.
- [70] X. Yuan, H. Wang, Y. Wu, G. Zeng, X. Chen, L. Leng, Z. Wu, H. Li, *Appl. Organomet. Chem.* 30 (2016) 289–296.
- [71] A. Li, P. Zhang, X. Chang, W. Cai, T. Wang, J. Gong, *Small* 11 (2015) 1892–1899.